Electrochimica Acta 56 (2011) 9818–9823

Contents lists available at SciVerse ScienceDirect

Electrochimica Acta

journal homepage: www.elsevier.com/locate/electacta

Electrochemical and interfacial behavior of a $FeSi_{2.7}$ thin film electrode in an ionic liquid electrolyte

Ji-Ae Choi [a], Dong-Won Kim [a,*], Young-San Bae [b], Seung-Wan Song [b], Soo-Hyung Hong [c], Sung-Man Lee [c]

[a] Department of Chemical Engineering, Hanyang University, Seoul 133-791, Republic of Korea
[b] Department of Fine Chemical Engineering & Applied Chemistry, Chungnam National University, Daejeon 305-764, Republic of Korea
[c] Department of Advanced Materials Science and Engineering, Kangwon National University, Kangwon-Do 200-701, Republic of Korea

ARTICLE INFO

Article history:
Received 13 April 2011
Received in revised form 9 August 2011
Accepted 16 August 2011
Available online 30 August 2011

Keywords:
Ionic liquid
Si-based anode
Si–Fe alloy
Lithium-ion battery
SEI layer

ABSTRACT

A $FeSi_{2.7}$ thin film is deposited on a copper substrate by RF magnetron sputtering of a Fe–Si alloy target. The electrochemical behavior of the $FeSi_{2.7}$ electrode in ionic liquid electrolyte based on 1-butyl-1-methylpyrrolidinium bis(trifluoromethanesulfonyl) imide is investigated and compared with that of a $FeSi_{2.7}$ electrode in conventional liquid electrolyte. The $FeSi_{2.7}$ electrode in the ionic liquid electrolyte delivers an initial discharge capacity of 756 mAh g^{-1} at room temperature, and its discharge capacity is maintained to be 92% of the initial discharge capacity after the 100th cycle. AC impedance and FTIR analysis reveal that the formation of a stable solid electrolyte interphase (SEI) layer on the $FeSi_{2.7}$ electrode in the ionic liquid electrolyte leads to a good capacity retention. This study demonstrates that the $FeSi_{2.7}$ electrode exhibits stable cycling behavior and good interfacial characteristics in the ionic liquid electrolyte without any solvents and additives.

1. Introduction

Silicon is an attractive anode material owing to its large theoretical charge capacity, particularly when compared to that of graphite, which is an active anode material currently used in lithium-ion batteries. However, silicon undergoes a substantial volume change during Li insertion and extraction reactions, which causes a mechanical failure of the active material, and thus results in poor cycling stability of the electrode [1–4]. Many attempts have been made to overcome this problem. Among them, the use of Si-transition metal alloy electrodes has attracted much attention because of their high volumetric capacity and good capacity retention [5–13]. The silicon alloys consist of an active Si phase in an inactive matrix, in which the Si phase with small volume changes should be uniformly distributed in the inactive matrix, thereby accommodating the volume change and improving the cycling stability.

Recently, ionic liquids have been intensively studied as safe electrolytes for lithium-ion batteries because of their non-flammability as well as their high electrochemical and thermal stabilities [14,15]. Among the various ionic liquid systems, those based on pyrrolidinium cations and bis(trifluoromethanesulfonyl) imide anions are considered promising for battery application, owing to their wide electrochemical stability and high ionic conductivity [16,17]. Accordingly, several electrochemical investigations of pyrrolidinium-based ionic liquids have been reported in the literature [16–23]. However, to our knowledge, there are few reports on the studies of the electrochemical behavior of silicon alloy electrodes in pyrrolidinium-based ionic liquid electrolytes [23]. The complicated and inscrutable interfacial reactions between the Si-based anode and the ionic liquid electrolyte are likely the cause of this limited attention. Surface characterization of silicon alloy-based thin film electrodes using infrared (IR) spectroscopy can provide direct information on the functional groups of the solid electrolyte interphase (SEI) without interfering signals from carbon and polymer binder additives, which could provide insight into the electrode–electrolyte interfacial behavior.

For this work, we prepared thin film $FeSi_{2.7}$ electrodes via RF magnetron sputtering of Si–Fe alloy target. The electrochemical performance of a $FeSi_{2.7}$ electrode in ionic liquid electrolyte based on 1-butyl-1-methylpyrrolidinium bis(trifluoromethanesulfonyl) imide (BMP-TFSI) was evaluated and compared with the performance of a $FeSi_{2.7}$ electrode in conventional liquid electrolyte by using galvanostatic cycling tests and AC impedance spectroscopy. The $FeSi_{2.7}$ electrode showed better capacity retention in both conventional liquid electrolyte and ionic liquid electrolyte than the Si–Cu electrode that exhibited a rapid capacity fade within 10 cycles in conventional electrolyte [23]. The SEI layer formed on the $FeSi_{2.7}$ film electrode during cycling was also investigated by *ex-situ* attenuated total reflection (ATR) FTIR spectroscopy.

* Corresponding author. Tel.: +82 2 2220 2337; fax: +82 2 2298 4101.
E-mail address: dongwonkim@hanyang.ac.kr (D.-W. Kim).

0013-4686/$ – see front matter © 2011 Elsevier Ltd. All rights reserved.
doi:10.1016/j.electacta.2011.08.080

2. Experimental

2.1. Preparation and characterization of the thin film $FeSi_{2.7}$ electrode

A Fe–Si thin film was deposited on a copper substrate by RF magnetron sputtering of an alloy target. The surface of the Cu substrate was modified by etching it with an aqueous solution of $FeCl_3$ and HCl (5 g $FeCl_3$/15 ml HCl/60 ml H_2O) for 1 min. The Fe–Si alloy target was prepared by mechanical alloying of the elemental powders of Fe and Si, followed by cold compaction and sintering at 1100 °C for 2 h under an argon atmosphere. The mechanical alloying was performed using a SPEX-8000 high energy ball mill with stainless steel balls and vial inside an argon-filled glove box. The deposition chamber was pumped down to a base pressure of 2×10^{-6} Torr and the working pressure was kept at 5 mTorr. The thickness of the film electrode was about 180 nm. Composition analysis for the thin film electrode was carried out by energy-dispersive spectroscopy (EDS). The structural identification of the Si–Fe alloy was performed by X-ray diffraction (XRD) and transmission electron microscopy (TEM).

2.2. Cell assembly and measurements

The BMP-TFSI was purchased from Chem Tech Research Incorporation and dried under a vacuum at 100 °C for 24 h before use. The water content in BMP-TFSI after drying was determined to be 8 ppm by Karl Fischer titration. An ionic liquid electrolyte was prepared by dissolving 1.0 M of lithium bis(trifluoromethanesulfonyl) imide (LiTFSI) in BMP-TFSI. LiTFSI was used as a lithium salt, since it was suitable for ionic liquid containing TFSI anion. The liquid electrolyte used for comparative purposes (henceforth referred to as the conventional liquid electrolyte) was 1.0 M $LiPF_6$ in ethylene carbonate (EC)/diethyl carbonate (DEC) (1:1 by volume, Techno Semichem Co., Ltd., battery grade), which has been one of the most common electrolyte systems used in lithium-ion batteries. The coin cell (CR2032) composed of a lithium metal, a polypropylene separator (Celgard 2400) and a $FeSi_{2.7}$ electrode was assembled with the ionic liquid electrolyte or the conventional liquid electrolyte in a dry box filled with argon gas. Charge and discharge cycling tests of the cells were conducted at a current density of 20 μA cm^{-2} (0.3C rate) over a voltage range of 0–1.2 V with battery test equipment. The AC impedance measurements were performed using an impedance analyzer over the frequency range of 1 mHz to 100 kHz with an amplitude of 10 mV.

2.3. Surface characterization

Changes in the surface morphology of $FeSi_{2.7}$ electrodes before and after cycling were characterized using a scanning electron microscope (SEM, JEOL JSM-6300). Surface characterization of the cycled $FeSi_{2.7}$ electrodes was conducted via *ex-situ* ATR-FTIR spectroscopy using an IR spectrometer equipped with a mercury–cadmium–telluride detector. The residual electrolyte was removed from the cycled electrode by washing thoroughly in dimethyl carbonate (DMC) prior to collecting the IR spectrum. Note that soluble species could be removed by the DMC washing. Since the electrodes were directly mounted on the closed single-reflection ATR unit with a Ge optic in the Ar-filled glove box, there was no moment of atmospheric contamination for the samples during transportation to the IR instrument as well as during the IR measurement. A total of 512 scans were co-added with a spectral resolution of 4 cm^{-1}. The spectra were corrected for the light penetration depth as a function of wavelength.

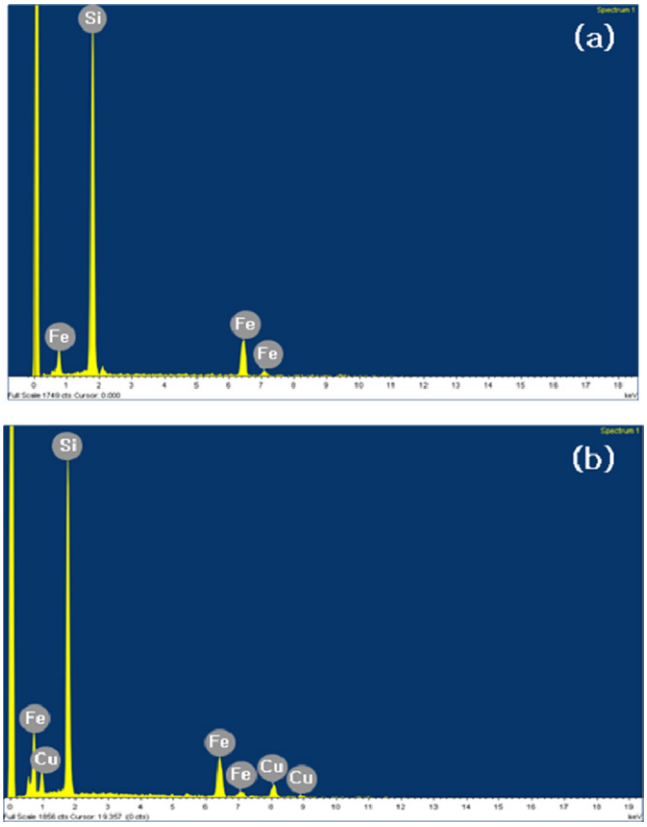

Fig. 1. EDS results of (a) the Fe–Si alloy target and (b) the as-deposited Fe–Si thin film electrode.

3. Results and discussion

The EDS data for the alloy target and the as-deposited Fe–Si thin film electrode are compared in Fig. 1. Additional Cu peaks from the substrate are observed in the as-deposited Fe–Si thin film electrode. The composition of the as-deposited Fe–Si thin film was estimated to be $FeSi_{2.72}$ from the EDS analysis, which is similar to that of the sputtering alloy target ($FeSi_{2.70}$). XRD pattern of the $FeSi_{2.7}$ film deposited on the Cu substrate was compared with that of the target, as shown in Fig. 2. The pattern for the thin film shows a significantly broad feature of reflections, compared to that of target corresponding to the orthorhombic (*Cmca*) structure of $FeSi_2$ [24]

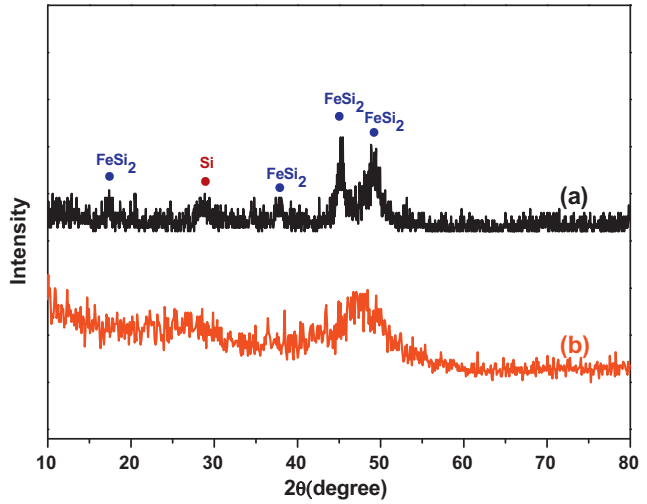

Fig. 2. XRD patterns of (a) the Fe–Si alloy target and (b) the as-deposited Fe–Si thin film.

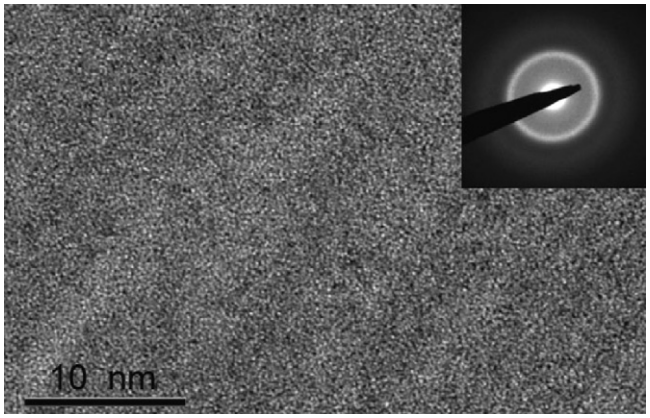

Fig. 3. High resolution TEM image of the as-deposited Fe–Si film.

and the cubic Si. The peak broadening observed for the film may be associated with amorphous-like structure of the film. Fig. 3 shows the high resolution TEM image of the as-deposited $FeSi_{2.7}$ film. A featureless modulated contrast without appreciable periodicity is observed, indicating that the as-deposited film consists of amorphous structure, which is consistent with the XRD result. The selected area diffraction pattern also consists of only amorphous like halo.

Fig. 4 shows the charge and discharge curves of the thin film $FeSi_{2.7}$ electrode in different electrolytes for the first and second cycles. The two electrolyte systems exhibit typical charge and discharge profiles corresponding to the lithiation of Si (forming Li_xSi) and the delithiation of Li_xS (regenerating Si), respectively. For the conventional liquid electrolyte, the initial charge and discharge capacities were 1442 and 1073 mAh g^{-1} based on the $FeSi_{2.7}$ electrode (this mass includes both Si and Fe), respectively, with an efficiency of 74.4%. The discharge capacity decreased to 1060 mAh g^{-1} and the efficiency increases 89.3% during the second cycle. On the other hand, the initial discharge capacity of the $FeSi_{2.7}$ electrode in the ionic liquid electrolyte was 756 mAh g^{-1} with an efficiency of 65.8%. The lower initial discharge capacity of the $FeSi_{2.7}$ electrode in ionic liquid electrolyte can be explained by considering that the use of an ionic liquid electrolyte causes an increase in viscosity, which results in an increase of the resistance for ion migration in the electrolyte and charge transfer reaction on the $FeSi_{2.7}$ electrode. Both the discharge capacity and the efficiency increased to 766 mAh g^{-1} and 91.8% during the second cycle. Higher efficiency at the second cycle as compared to that of cell with liquid electrolyte (89.3%) indicates that the reductive decomposition of ionic liquid electrolyte was suppressed by SEI layer formed at the first cycle. Differential capacity plots shown in Fig. 5 give a better peak resolution for Si reaction and electrolyte decomposition, respectively. In the liquid electrolyte, the first cathodic process shows a small peak ranged from 0.65 to 0.32 V, which is associated with reductive decomposition of electrolyte components, as previously reported in Si electrodes [25,26]. Significant cathodic peak below 0.2 V is due to the lithiation of Si. At the second cycle, the peak observed near 0.43 V disappeared, but the reductive decomposition occurred around 0.35 V. This might be caused by reductive electrolyte decomposition due to the ineffective coverage of the thin film electrode with SEI formed at the first cycle. The first charge process in ionic liquid electrolyte shows a similar feature to the electrode in conventional liquid electrolyte with a rather broad reductive peak ranged from 0.70 to 0.30 V, which is attributable to the reductive decomposition of ionic liquid electrolyte. It should be noted that the reductive decomposition below 0.30 V at the second cycle was significantly reduced in ionic liquid electrolyte. This result indicates the effective formation of an SEI layer on the $FeSi_{2.7}$ electrode during first cycle, which prevents the reductive decomposition of the ionic liquid electrolyte for consecutive cycling.

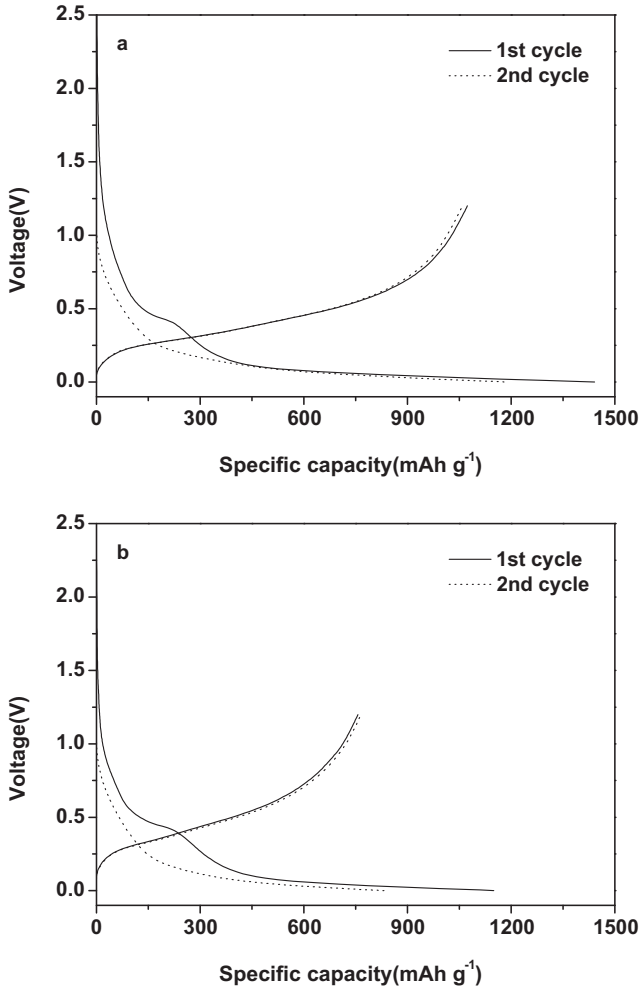

Fig. 4. Charge and discharge curves of the thin film $FeSi_{2.7}$ electrode in different electrolytes during the first and second cycles: (a) conventional liquid electrolyte and (b) ionic liquid electrolyte. Cycling was carried out between 0 and 1.2 V at a current density of 20 μA cm^{-2} (0.3C rate).

Fig. 6 shows the discharge capacities of the $FeSi_{2.7}$ electrode in the conventional liquid electrolyte and the ionic liquid electrolyte as a function of cycle number. The discharge capacity of the $FeSi_{2.7}$ electrode in the ionic liquid electrolyte declined to 694 mAh g^{-1} after the 100th cycle, which corresponds to 92% of the initial discharge capacity, whereas the capacity retention of the $FeSi_{2.7}$ electrode in the conventional liquid electrolyte was 73%. The difference in the capacity retention behaviors of the two electrolyte systems may have arisen from the different interfacial characteristics of the $FeSi_{2.7}$ electrode during cycling.

In order to investigate the interfacial behavior of the $FeSi_{2.7}$ electrode during cycling, the AC impedance of the cells was measured while the cell was in the discharged state after 1st and 100th cycles, respectively. The resultant AC impedance spectra are shown in Fig. 7. All the spectra are composed of a semicircle in a high-frequency range and a straight line with a slope of approximately 45° in a low-frequency region. These spectra can be analyzed by using the equivalent circuit given in Fig. 7b. The high frequency semicircle is associated with the overall interfacial resistance (R_i), which consists of the resistance of the SEI film formed on the electrode surface and the charge transfer resistance, and the straight line with the 45° slope at low frequencies can be ascribed to the Warburg diffusion of lithium ions in the thin $FeSi_{2.7}$ electrode.

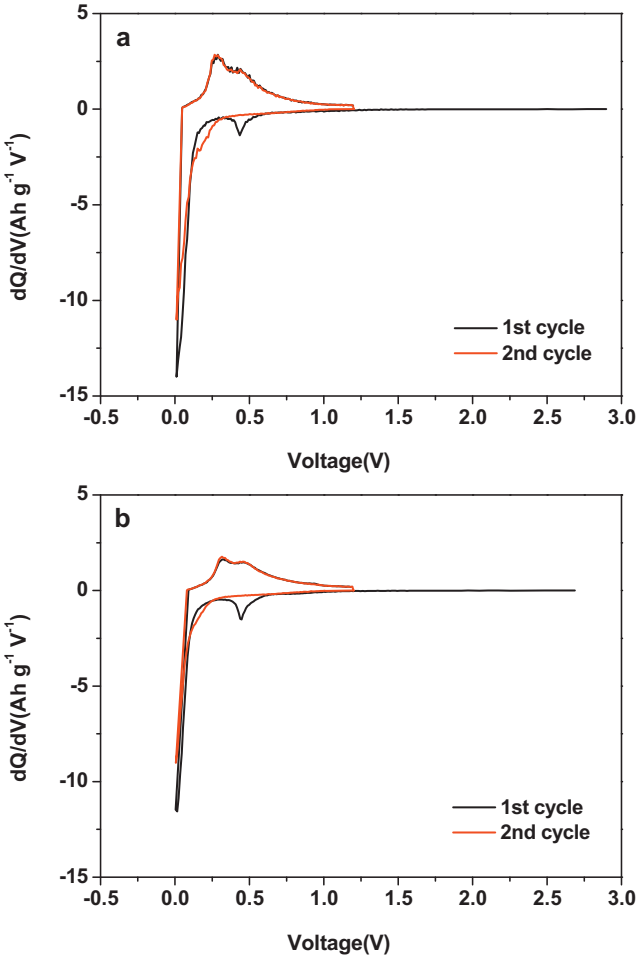

Fig. 5. Differential capacity *vs.* potential curves of the thin film $FeSi_{2.7}$ electrode in different electrolytes during the first and second cycles: (a) conventional liquid electrolyte and (b) ionic liquid electrolyte.

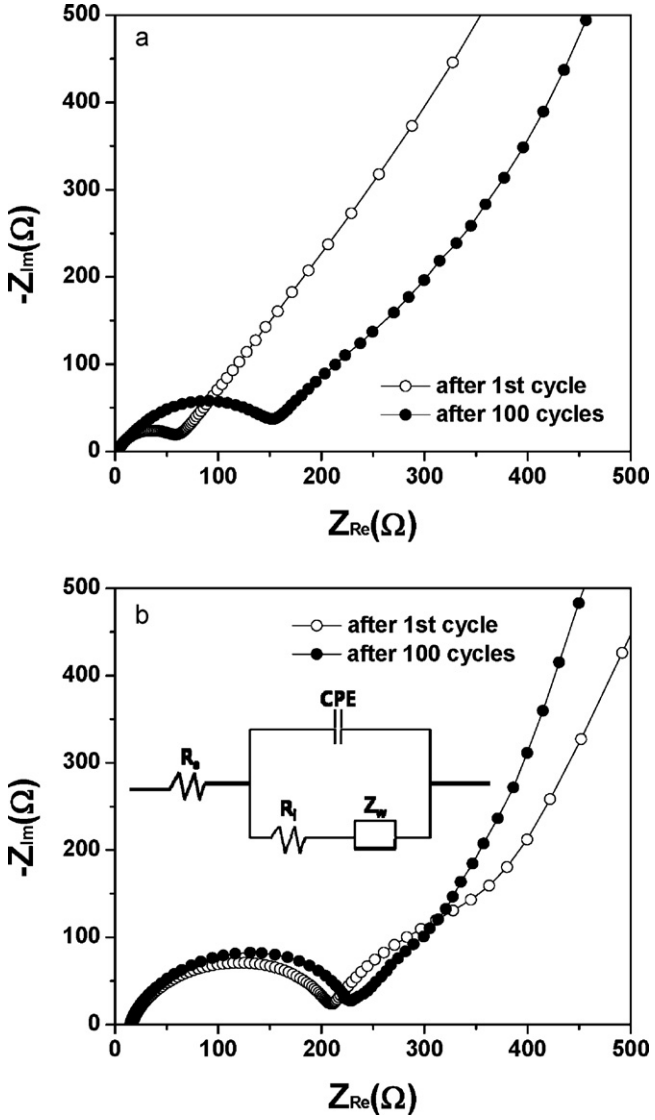

Fig. 7. AC impedance spectra of the $FeSi_{2.7}$ electrode in (a) the conventional liquid electrolyte and (b) the ionic liquid electrolyte, obtained at the fully discharged state after the first and 100th cycles. The inset shows the equivalent circuit.

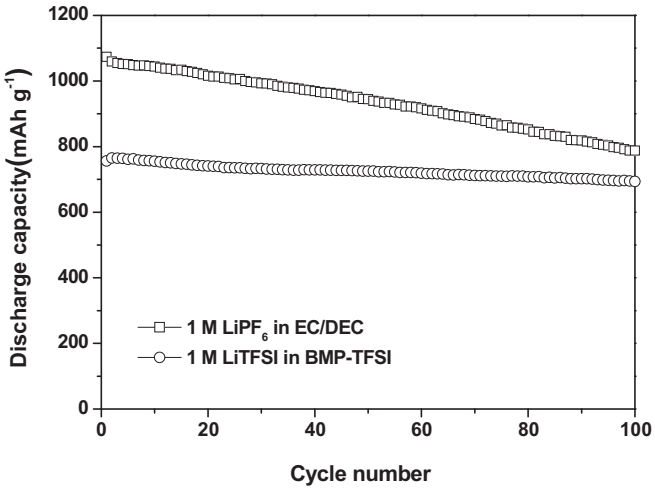

Fig. 6. Discharge capacities of the thin film $FeSi_{2.7}$ electrodes in the conventional liquid electrolyte (1 M $LiPF_6$ in EC/DEC) and ionic liquid electrolyte (1 M LiTFSI in BMP-TFSI), as a function of cycle number. Cycling was carried out between 0 and 1.2 V at a current density of 20 $\mu A\,cm^{-2}$ (0.3C rate).

[27,28]. The electrolyte resistances (R_s) could be also estimated from the high frequency intercepts of the real axis. As expected, the electrolyte resistance of ionic liquid electrolyte (15.9 Ω) was higher than that of conventional liquid electrolyte (3.1 Ω), due to the viscous nature of ionic liquid electrolyte. In the conventional liquid electrolyte, the interfacial resistance significantly increased from 55.2 to 149.4 Ω after 100 cycles. On the contrary, the interfacial resistance was little changed after the 100th cycle in the ionic liquid electrolyte (from 192.5 to 213.4 Ω), even though the absolute value of the interfacial resistance was slightly higher than that in the conventional liquid electrolyte. This result suggests that a highly stable SEI film on the $FeSi_{2.7}$ electrode formed in the early stages of cycling in the ionic liquid electrolyte, thereby inhibiting a further irreversible reaction of the electrolyte and resulting in the stable cycling behavior shown in Fig. 6.

Fig. 8 shows the surface morphology of the $FeSi_{2.7}$ electrode before and after cycled (100 cycles) in different electrolyte systems. The surface of the as-deposited film was covered with small particles in part of the film, as shown in Fig. 8a. After cycling in conventional liquid electrolyte, the surface of the film was rough and covered with deposits of SEI products. The deposits look more

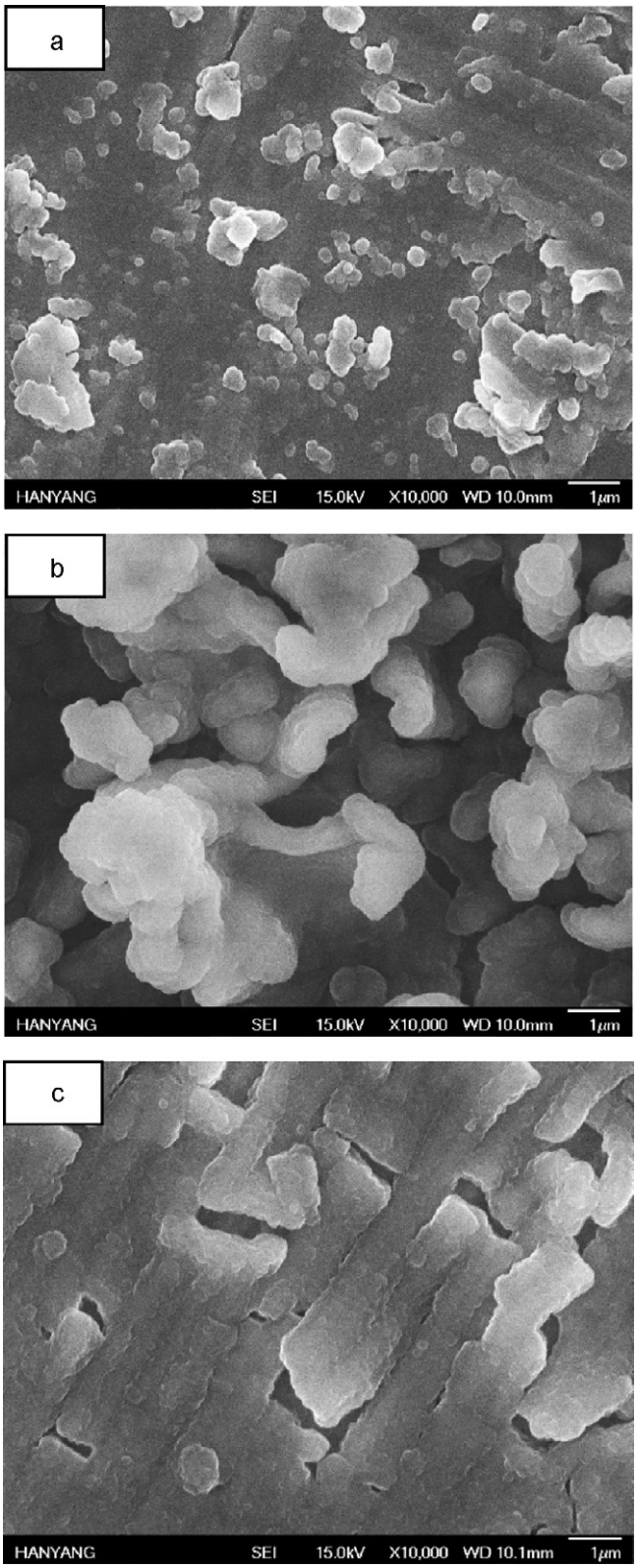

Fig. 8. SEM images of the $FeSi_{2.7}$ electrode surface before and after cycled in different electrolyte systems: (a) before cycling, (b) after 100 cycling in the conventional liquid electrolyte and (c) the ionic liquid electrolyte.

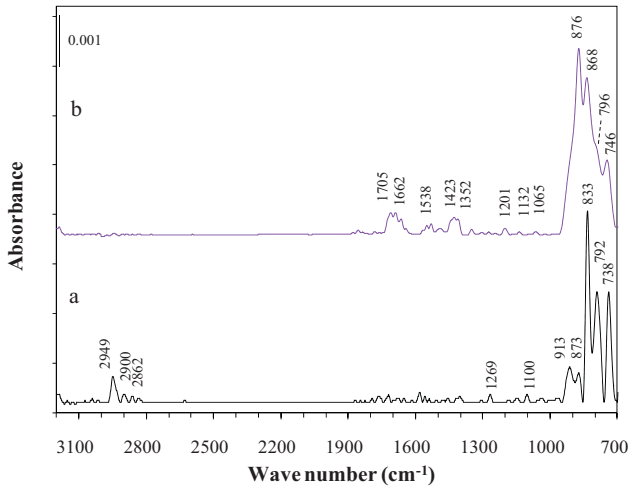

Fig. 9. IR spectral comparison of the surface of the $FeSi_{2.7}$ electrodes obtained after 100 cycles in (a) the conventional liquid electrolyte and (b) the ionic liquid electrolyte.

separated each other and appear to have less connectivity among them. In contrast, the SEI layer formed on the electrode cycled in ionic liquid electrolyte almost completely covered the film electrode. The deposits look connected each other. The effective coverage of the electrode prevents the reductive decomposition of the ionic liquid electrolyte for consecutive cycling, as explained in Fig. 5, and thus leads to good capacity retention, as shown in Fig. 6.

The surface of the cycled $FeSi_{2.7}$ electrode was analyzed using *ex-situ* ATR FTIR spectroscopy. Fig. 9 compares the IR spectra of the surface of the $FeSi_{2.7}$ electrodes obtained in different electrolytes after 100 cycles. The surface of the electrode in the conventional liquid electrolyte (Fig. 9a) exhibits mainly multiple peaks in the region of 920–730 cm^{-1}, which can be attributed to the P-F group and the M-F group (M = Si/Fe). The peaks observed at 913 and 873 cm^{-1} can be assigned to the Si–F group [29]. Tiny peaks at 1269, below 1100, and at 833 cm^{-1} can be attributed to the P═O, the P–O–C and the P–F groups, respectively, and are from O═PF–OR compounds. In fact, they may have originated from the decomposition of PF_6^--derived species. The peaks appearing at 2950–2840 cm^{-1} are characteristic of the CH_3CH_2-alkyl group, which are the decomposition products of ethylene carbonate (EC), diethyl carbonate (DEC) and their derivatives. In Fig. 9b, the electrode surface after cycling in the ionic liquid electrolyte shows weak absorbance peaks near 1705–1662 cm^{-1} owing to the C═O group of ester $-CO_2-R$ or alkyl carbonate salt $R-OCO_2^-M^{n+}$ (M = Li/Si), together with fingerprints at 1423, 1352, 1201, 1132 and 796 cm^{-1}. Very tiny peaks at 1565 cm^{-1} indicate the trace of carboxylate metal salt $R-CO_2^-M^{n+}$. These organic species are the BMP decomposition products, perhaps coupled with oxygen from the TFSI anion and surface oxygen of the electrode. Other tiny peaks near 1201 cm^{-1} can be attributed to the C–F group, while those at 1065 and 796 cm^{-1} may be associated with the SNS group, and the one at 746 cm^{-1} with the –CS– group from the TFSI decomposition. Overlapping peaks of –CF, –SNS–, SO_3^{2-} and M–F below 900 cm^{-1} appear to enhance the peaks' absorbance. The above IR data analysis shows that the surface of the $FeSi_{2.7}$ electrode cycled in the conventional liquid electrolyte was mostly composed of PF_6^- decomposition products. Continued capacity loss (see Fig. 6) and an increase in interfacial resistance (see Fig. 7a) indicate that the uncovered part of the electrode surface was subjected to either further irreversible reactions [30] or the deactivation of the Si by PF_6^- decomposition products [31]. On the other hand, the electrode in the ionic liquid electrolyte contained a relatively low concentration level of the decomposition products of both the BMP cation and the TFSI anion, which

may be correlated with an improved capacity retention and little change in the interfacial resistance when using an ionic liquid electrolyte for more than 100 cycles. Thus, an ionic liquid electrolyte seems to effectively passivate the electrode surface in the early stages of cycling despite a very thin or low concentration level of SEI species.

4. Conclusions

The thin film $FeSi_{2.7}$ electrode was prepared by RF magnetron sputtering of a Si–Fe alloy target. The electrochemical behavior of the $FeSi_{2.7}$ electrode was investigated in an ionic liquid electrolyte (1.0 M in BMP-TFSI) without any solvent molecules. The electrode in the ionic liquid electrolyte exhibited a stable and reversible cycling behavior, which was comparable to that observed in a common liquid electrolyte. AC impedance and FTIR analysis demonstrated that a very stable SEI layer effectively passivated the $FeSi_{2.7}$ electrode surface in the early stages of cycling, inhibiting further decomposition of the electrolyte at the electrode surface. It is thus expected that the combination of the ionic liquid electrolyte and the Si-based anode can facilitate a safe lithium-ion battery with high capacity and good capacity retention.

Acknowledgements

This work was supported by the National Research Foundation (NRF) of Korea Grant, funded by the Korea government (MEST) (2010-0027665 and NRF-2009-C1AAA001-0093307). This research was also supported by a Grant from the Fundamental R&D Program for Core Technology of Materials, funded by the Ministry of Knowledge Economy, Korea

References

[1] S.J. Lee, J.K. Lee, S.H. Chung, H.Y. Lee, S.M. Lee, H.K. Baik, J. Power Sources 97–98 (2001) 191.
[2] M.N. Obrovac, L. Christensen, Electrochem. Solid-State Lett. 7 (2004) A93.
[3] U. Kasavajjula, C. Wang, A.J. Appleby, J. Power Sources 163 (2007) 1003.
[4] M.N. Obrovac, L.J. Krause, J. Electrochem. Soc. 152 (2007) A103.
[5] G.X. Wang, L. Sun, D.H. Bradhurst, S. Zhong, S.X. Dou, H.K. Liu, J. Alloy Compd. 306 (2000) 249.
[6] J.B. Kim, H.Y. Lee, K.S. Lee, S.H. Lim, S.M. Lee, Electrochem. Commun. 5 (2003) 544.
[7] H. Dong, R.X. Feng, X.P. Ai, Y.L. Cao, H.X. Yang, Electrochim. Acta 49 (2004) 5217.
[8] M.S. Park, Y.J. Lee, S. Rajendran, M.S. Song, H.S. Kim, J.Y. Lee, Electrochim. Acta 50 (2005) 5561.
[9] J.H. Kim, H. Kim, H.J. Sohn, Electrochem. Commun. 7 (2005) 557.
[10] B.C. Kim, H. Uono, T. Satou, T. Fuse, T. Ishihara, M. Ue, M. Senna, J. Electrochem. Soc. 152 (2005) A523.
[11] Y.S. Lee, J.H. Lee, Y.W. Kim, Y.K. Sun, S.M. Lee, Electrochim. Acta 153 (2006) 1523.
[12] T. Kim, S. Park, S.M. Oh, Electrochem. Commun. 8 (2006) 1461.
[13] K.M. Lee, Y.S. Lee, Y.W. Kim, Y.K. Sun, S.M. Lee, J. Alloy Compd. 472 (2009) 461.
[14] M. Armand, F. Endres, D.R. MacFarlane, H. Ohno, B. Scrosati, Nature Mater. 9 (2009) 621.
[15] A. Lewandowski, A. Swiderska-Mocek, J. Power Sources 194 (2009) 601.
[16] A. Fernicola, F. Croce, B. Scrosati, T. Watanabe, H. Ohno, J. Power Sources 174 (2007) 342.
[17] P. Reale, A. Fernicola, B. Scrosati, J. Power Sources 194 (2009) 182.
[18] J.H. Shin, W.A. Henderson, G.B. Appetecchi, F. Alessandrini, S. Passerini, Electrochim. Acta 50 (2005) 3859.
[19] J.H. Shin, E.J. Cairns, J. Power Sources 177 (2008) 537.
[20] L. Larush, V. Borgel, E. Markevich, O. Haik, E. Zinigrad, D. Aurbach, J. Power Sources 189 (2009) 217.
[21] V. Borgel, E. Markevich, D. Aurbach, G. Semrau, M. Schmidt, J. Power Sources 189 (2009) 331.
[22] J. Hassoun, A. Fernicola, M.A. Navarra, S. Panero, B. Scrosati, J. Power Sources 195 (2010) 574.
[23] C.C. Nguyen, S.W. Song, Electrochem. Commun. 12 (2010) 1593.
[24] P.Y. Dusausoy, J. Protas, R. Wandji, B. Roques, Acta Crystallogr. B 27 (1971) 1209.
[25] C.K. Chan, R. Ruffo, S.S. Hong, Y. Cui, J. Power Sources 189 (2009) 1132.
[26] J. Graetz, C.C. Ahn, R. Yazami, B. Fultz, Electrochem. Solid-State Lett. 6 (2003) A194.
[27] T. Sugimoto, Y. Atsumi, M. Kono, M. Kikuta, E. Ishiko, M. Yamagata, M. Ishikawa, J. Power Sources 195 (2010) 6153.
[28] D. Aurbach, K. Gamolsky, B. Markovsky, Y. Gofer, M. Schmidt, U. Heider, Electrochim. Acta 47 (2002) 1423.
[29] G. Socrates, Infrared Characteristic Group Frequencies, Tables and Charts, 2nd ed., John Wiley & Sons, New York, 1994.
[30] S.W. Song, S.W. Baek, Electrochem. Solid-State Lett. 12 (2009) A23.
[31] N.S. Choi, K.H. Yew, K.Y. Lee, M. Sung, H. Kim, S.S. Kim, J. Power Sources 161 (2006) 1254.